Bulk Dislocation Core Dissociation Probed by Coherent X Rays in Silicon

V. L. R. Jacques,[1,2] S. Ravy,[2] D. Le Bolloc'h,[1] E. Pinsolle,[1,2] M. Sauvage-Simkin,[2] and F. Livet[3]

[1]*Laboratoire de Physique des Solides (CNRS-UMR 8502), Bât. 510, Université Paris-sud, 91405 Orsay cedex, France*

[2]*Synchrotron SOLEIL, L'Orme des merisiers, Saint-Aubin BP 48, 91192 Gif-sur-Yvette cedex, France*

[3]*Sciences et Ingénierie des Matériaux et Procédés, INP Grenoble CNRS UJF, BP 75, 38402 St Martin d'Hères Cedex, France*

(Received 25 November 2010; published 10 February 2011)

We report on a new approach to probe bulk dislocations by using coherent x-ray diffraction. Coherent x rays are particularly suited for bulk dislocation studies because lattice phase shifts in condensed matter induce typical diffraction patterns which strongly depend on the fine structure of the dislocation cores. The strength of the method is demonstrated by performing coherent diffraction of a single dislocation loop in silicon. A dissociation of a bulk dislocation is measured and proves to be unusually large compared to surface dislocation dissociations. This work opens a route for the study of dislocation cores in the bulk in a static or dynamical regime, and under various external constraints.

DOI: 10.1103/PhysRevLett.106.065502 PACS numbers: 61.72.Ff, 42.25.Kb, 61.72.Dd

Understanding the origin and behavior of topological defects in hard condensed matter is a challenging problem. Their study has always been of prime importance because of their crucial influence on a very large number of physical properties [1]. In materials science, plastic deformation is directly related to the mobility of dislocations. In semiconductors, their damaging effects on charge carriers lifetime and mobility strongly affect the electronic properties [2]. In charge density waves systems, the drift velocity may be related to the climbing of density wave dislocations [3,4]. More recently, supersolidity of ^{4}He has been suggested to be due to dislocation pinning [5,6].

Observing dislocations has always been a difficult task and only a few techniques can probe such a discontinuity of space. Transmission electron microscopy (TEM) is the most powerful technique to access the topology of dislocations [7], the associated long-range strain fields [8] and to probe their dynamics [9]. However, TEM is limited to thin samples and does not allow measurements in the bulk, in which the constraints for dislocation motion are different. X-ray topography can also probe bulk dislocations but with a much poorer resolution [10]. However, even with TEM the study of dislocation cores remains a challenge [11], especially in semiconductors [12].

We demonstrate in this Letter that coherent x-ray diffraction (CXRD) is particularly suited for dislocation studies. To go further than the first experiments on misfit [13] and charge-density-wave [14] dislocations, we used an approach that sheds light on isolated dislocation lines deep inside samples and provides valuable information about their fine structure. A bulk dislocation dissociation is studied, revealing an unusual behavior compared to dissociations found in thin samples. The possibility to perform CXRD at low-temperature or under high pressure [15] is a strong asset to study dislocations under extreme conditions.

This experiment takes advantage of the coherence of the x-ray beam, which is very sensitive to lattice phase shifts as the phase of the beam wave front is correlated over several micrometres [16]. The presence of a dislocation line in the coherently illuminated volume strongly affects the distribution of intensity around Bragg reflections. Indeed, dislocations induce a π lattice phase shift localized over only a few atomic planes [17], which results in a destructive interference at the Bragg location due to the out-of-phase volumes located on both sides of the dislocation line [18]. When the latter is in the middle of the illuminated volume, a minimum of intensity is detected at the Bragg position. CXRD is thus a technique of choice for the study of bulk dislocations in any kind of lattice [14,18].

To demonstrate the strength of the method, we present measurements performed on a single dislocation loop in silicon. From an experimental point of view, a coherent x-ray beam is the first necessary condition to be sensitive to dislocations. The key point for a good understanding of the coherent diffraction pattern is also to ensure that a single dislocation loop is probed by the x-ray beam. To do so, we take advantage of the characteristics of light propagation through a rectangular aperture a. In the Fresnel regime, the beam size remains almost constant up to a distance $d_{FF} = a^2/4\lambda$, and then diverges in the Fraunhofer regime with a constant angle (λ/a). If both sample and detector are inserted in the parallel beam regime (below d_{FF}), a topogram is obtained. A far-field coherent diffraction pattern is obtained when the detector is located in the diverging beam region (downstream of d_{FF}). The two regimes have been reached in turn in the present experiment by adjusting the slit aperture a and keeping the detector at a fixed position. The topographic mode first provides a large-field survey of the 100 μm dislocation loops in the bulk, allowing focusing on a single one. The far-field diffraction mode is then used to precisely probe the dislocation core with the microbeam.

The experiment has been carried out at the CRISTAL diffraction beam line of the synchrotron SOLEIL [19]. The

 © 2011 American Physical Society

sample is mounted on a six-circle diffractometer, and probed with a $\lambda = 1.7462$ Å (7.1 keV) beam generated by a U20 undulator and monochromatized with a Si(111) double crystal monochromator (DCM). Because of the small divergence of the U20 beam, the full Darwin width of the monochromator is not excited. Focusing devices are not used in order to preserve the parallelism of the beam requested by topography. Consequently, the DCM has been detuned at 50% of the rocking curve maximum in order to reject harmonics. This results in a quasi parallel beam with a band pass better than the regular value $\Delta\lambda/\lambda = 1.4 \times 10^{-4}$. Two sets of slits are inserted. The first one, called source slits in the following, defines the beam size at $D =$ 13 m before the sample. The second, called sample slits, are located 8 cm before the sample, and are either wide open for topography, or closed in order to select only the coherent part of the beam to perform CXRD. In the latter configuration, the source slits were opened at $S = 200 \times 200\ \mu\text{m}^2$ and the sample slits aperture a was either $7 \times 7\ \mu\text{m}^2$ or $5 \times 5\ \mu\text{m}^2$. The estimated transverse coherence length at the sample slits position is around 10 μm, so that a fully coherent beam is selected. The resulting separation distance between near-field and far-field regimes for the sample slits diffraction leads to $d_{FF} =$ 7 cm for $a = 7\ \mu$m or 4 cm for $a = 5\ \mu$m. A direct illumination ANDOR CCD camera with 13 μm pixel size is positioned 2.2 m after the sample, and provides a resolution $\Delta q = 2.13 \times 10^{-5}$ Å^{-1}. This setup leads to a 80% total degree of coherence [20].

A $18 \times 9 \times 0.5$ mm^3 (110) oriented silicon sample, grown by the Czochralski method was annealed for 35 h at 1100 °C in an oxygen atmosphere, yielding an oxygen concentration of 10^{18} cm^{-3}. Oxygen incorporation leads to the formation of two kinds of defects. Type 1 are stacking faults (SF) bounded by partial dislocation loops with Burgers vectors $\mathbf{b}_S = 1/3\langle 111\rangle$, and type 2 are perfect dislocation loops, with Burgers vectors $\mathbf{b}_P = 1/2\langle 110\rangle$. The latter are generally dissociated into two partial dislocations, having Burgers vectors $\mathbf{b}_1$ and $\mathbf{b}_2$ respectively, so that $\mathbf{b}_P = \mathbf{b}_1 + \mathbf{b}_2$. The partial dislocations are called glissile if their direction and Burgers vector belong to the same {111} glide plane, or sessile if not. A SF stands between the two partial dislocation lines [7] provided one at least is glissile. In between dislocations, the crystal quality was excellent as demonstrated by the 220 reflection 0.004° rocking curve width.

Reflection topography has first been performed on the 220 Bragg reflection by using a 1 μm grain Kodak Industrex M photographic film [Fig. 1(a)] to get a large field view of the dislocations in the sample. Among the several loops appearing in this region, an isolated one, 100 μm in diameter, was selected for further study [Fig. 1(b)].

The CXRD configuration was obtained by closing the sample slits down to 5 μm around a dislocation loop selected by topography. The 220 reflection is recorded while moving the sample with respect to the coherent beam in the two directions parallel to the surface with $5\ \mu\text{m} \times 5\ \mu\text{m}$ steps. Figure 2(a) shows a series of

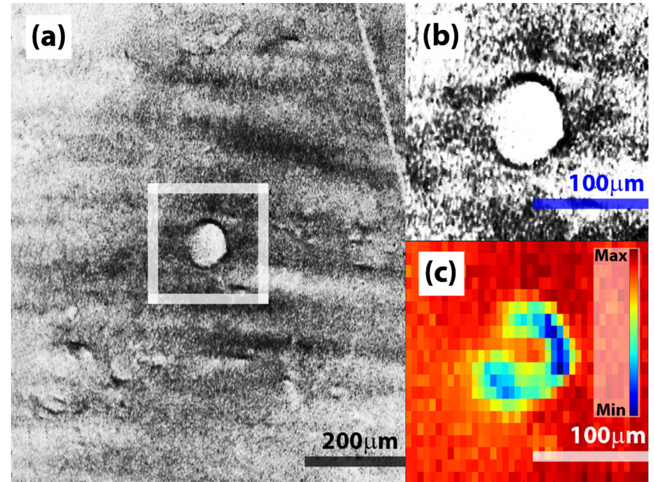

FIG. 1 (color online). (a) Reflection topography image taken on the 220 Bragg reflection, providing a large-field view of the dislocations in this region of the sample, and (b) zoom on the isolated dislocation in the middle of the image shown in (a). (c) Same dislocation imaged with a $7 \times 7\ \mu\text{m}^2$ coherent beam, obtained by taking at each position the intensity at the 220 Bragg reflection position.

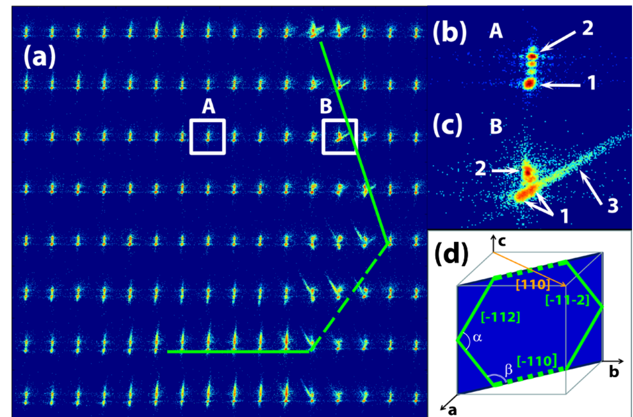

FIG. 2 (color online). (a) CXRD images recorded on the 220 reflection with $5 \times 5\ \mu\text{m}^2$ steps, with the sample detuned by 0.008° from the Bragg angle (log scale). Images A and B were recorded in a perfect region of the sample and at a dislocation line position, respectively. (b) CXRD pattern obtained in a perfect region of the sample (log scale). Arrow 1 points towards the CTR and arrow 2 towards the 220 reflections generated by the secondary beams coming from the sample slit diffraction fringes. (c) CXRD pattern obtained when a dislocation line is illuminated (log scale). The CTR is split, and an additional streak appears (3). (d) Geometry of the sample surface plane and of the dislocation lines propagation directions. Solid and dashed lines refer to the same directions as in (a). $\alpha = 109.47°$ and $\beta = 125.26°$.

measurements taken in the region of a type 2 perfect dislocation loop with the sample detuned by 0.008° from the 220 Bragg angle to avoid its highly intense maximum. In these conditions, the typical image obtained in a perfect region of the sample is shown in Fig. 2(b). To interpret this image, one has to consider the diffraction by the sample slits which gives rise to interference fringes in both horizontal and vertical directions acting as secondary incident beams. For the mth fringe, the angular deviation with respect to the main beam is $\pm(m + 1/2)\lambda/a$ ($\lambda/a = 35\ \mu$rad). As the Darwin width of the 220 reflection is 30 μrad, only one fringe is Bragg diffracted at a time in the vertical plane. In the horizontal one, the actual incident angle projected onto the scattering plane is changed by a much smaller value of $\sim 1 \times 10^{-9}$ rad and the simultaneous reflection of many fringes is possible [Fig. 3(a)]. When the crystal is detuned by $0.008° \sim 140\ \mu$rad, the crystal truncation rod (CTR) gives a maximum of intensity indicated by arrow 1 in Fig. 2(b). The secondary beam of order $m = 3$ is Bragg diffracted [arrow 2 in Fig. 2(b)]. The CTRs from $m = 1$ and 2 fringes are visible in between. Because of the narrow divergence of the primary beam, no monochromator streak [21] is detected. In addition, a possible radial streak induced by the wavelength spread would be hidden by the CTR. Figure 2(c) shows the typical CXRD image obtained when the beam illuminates a dislocation line. The diffraction pattern looks very different compared to the ones obtained in perfect regions. A splitting appears on the CTR, indicating that the Bragg reflection is also split. The splitting of the Bragg reflection itself at the exact Bragg incident angle is clearly visible in Fig. 3(a). As discussed in the introduction, this splitting is due to the dislocation induced destructive interference *at* the Bragg reflection position.

A direct imaging method based on the characteristic shape of the diffraction pattern corresponding to a dislocation line is proposed here, consisting in assigning to each position of the sample the intensity at the Bragg position. By doing so one finds minima only at the dislocation line position. Figure 1(c) is the result obtained with this method in the region of the dislocation loop shown in Fig. 1(b). The dislocation loop line appears clearly, and is in good agreement with the image obtained with topography. An important point of this measurement is that the resolution of the imaging depends on the beam size. In that sense, the resolution achievable with this method could be decreased to few nanometers with high quality focusing optics [22], going well beyond topography, limited by the best resolution of presently available detectors (1 μm for photographic films or specially designed CCD cameras [23]).

Much more information can be extracted from the diffraction patterns about the fine structure of the dislocation cores. The imaging techniques produce direct images of real space while by CXRD, a distribution of intensity in reciprocal space is obtained. Therefore, the resolution is

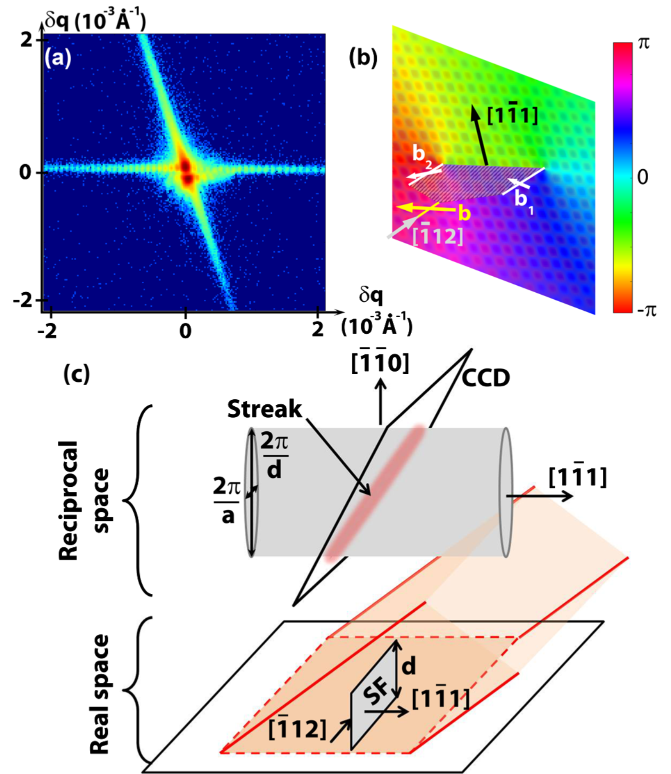

FIG. 3 (color online). (a) Measured CXRD pattern of the 220 at a dislocation line position (log scale). The Bragg reflection is split, and a streak along the $\langle 1\bar{1}1\rangle$ direction appears. Horizontal fringes correspond to the secondary beams due to the diffraction of the sample slits. (b) Schematic representation of a dissociated dislocation corresponding to the diffraction pattern shown in (a). Burgers vector of the perfect dislocation (yellow): $\mathbf{b} = 1/2[\bar{1}\,\bar{1}\,0]$, and of the two partials in the dissociated case (white): $\mathbf{b}_1 = 1/6[\bar{2}\,\bar{1}\,1]$ and $\mathbf{b}_2 = 1/6[\bar{1}\,\bar{2}\,\bar{1}]$. The hatched plane between the parallel partial dislocations is a SF ribbon. The color scale represents the value of the phase around the dissociated dislocation. A schematic lattice is shown in the background. (c) Schematic of the dissociated dislocation illuminated by a coherent beam (represented in orange). The dislocation lines are along $[\bar{1}12]$, Burgers vectors along $\mathbf{b}_1$ and $\mathbf{b}_2$ and the SF lies in the $(1\bar{1}1)$ plane. The corresponding reciprocal space distribution is shown around the 220 reflection. The signal corresponding to the stacking fault is a cylinder with ellipsoidal cross section. The ellipse semi-axis lengths are inversely proportional to a and d along $[\bar{1}12]$ and $[\bar{1}\,\bar{1}\,0]$ respectively. The cut of the Ewald sphere through the cylinder produces the streak observed.

given in terms of wave vector, inversely proportional to space resolution which makes the detection of fine structures clearer.

One can see in Fig. 2(a) that a diffuse streak appears when the beam illuminates the dislocation line. This streak is perpendicular to the dislocation line, always along the projection of a $\langle 111\rangle$ direction onto the cut plane of the CCD. The fact that the streak appears only at the dislocation line position (and not when the beam probes inside the loop) and always lies along a $\langle 111\rangle$ direction is a strong indication that this scattering comes from the SF

lying between the partials of the dissociated dislocation. As shown in Fig. 3(a), the streak is also visible at the Bragg angle, and corresponds to the geometry of a dissociated dislocation schematically represented in Fig. 3(b). Hence, dislocation dissociations are visible with x-ray microbeams, while they are not by topography.

Some quantitative information can be extracted out of our measurements. The transverse widths of the streak are inversely proportional to the transverse sizes of the SF which is a very thin ribbon perpendicular to the SF plane, elongated in the direction of the dislocation lines, and with a finite size d between the partials. The corresponding signal in Fourier space is also a ribbon, elongated perpendicular to the SF, and with finite sizes in the two other directions. One is driven by the beam size a, and the other is inversely proportional to d. Figure 3(c) is a schematic of the real space configuration of the beam probing a dissociated dislocation and of the corresponding distribution in reciprocal space.

On the diffraction patterns, the streak has the same width as the Bragg reflection in the direction of the dislocation line, as expected. The elongated direction width should be inversely proportional to the separation between the partials d. But surprisingly, whatever its direction, the streak is found much shorter than expected from the usual separation of a few nanometers measured in TEM [7]. A few nanometers dissociation would produce a streak expanding over several times the size of the detector. Here, the streak spreads over an angle corresponding to much larger distances, of several hundred nanometers. This disagreement between CXRD and TEM could be due to the small penetration length of electron beams. Only surface dislocations are probed by electrons, in contrast to the present work which describes a dissociated dislocation in the bulk. Although the discrepancy seems particularly large, it is interesting to note that relatively large dissociations were already observed by TEM, as reported in Ref. [24]. It is emphasized in this work that large dissociations always occur in thicker parts of the sample, i.e., 3 times the extinction length. As our sample is 0.5 mm thick, the dissociations could then be larger than in thin samples. In any case, further studies have to be devoted to this effect, by recording the three dimensional distribution of intensity of the streak around the 220 reflection.

As a conclusion, we have presented a new approach to study phase defects including dislocations. CXRD allows dislocation imaging, and can provide improved resolution of bulk defects in comparison with existing techniques. Moreover, we show that the technique is sensitive to the structure of the dislocation through the first evidence of bulk dislocation dissociations. The distance between the partials is found to be much larger than in thin samples, which has to be confirmed by further studies. Ptychography [25] could also be performed on this kind of defect, though the π phase shift would most probably make the reconstruction algorithm convergence difficult. This work opens new perspectives for the study of bulk dislocations with coherent x rays, especially the strain [26,27] and the dynamics, combining coherence to variable parameters as pressure [15], temperature or stress, using an x-ray photon correlation spectroscopy approach.

The authors acknowledge G. Rolland for providing the sample, F. Picca for his help during experiments, B. Devincre for an illuminating discussion, and T. Schülli and P. G. Evans for their careful reading of the manuscript.

*Present address: European Synchrotron Radiation Facility, 6 rue Jules Horowitz, BP220, 38043 Grenoble Cedex, France.
vjacques@esrf.fr

[1] J. P. Hirth and J. Lothe, *Theory of Dislocations* (McGraw-Hill, New York, 1968).
[2] J. Kundu, C. Sarkar, and P. Mallick, Semicond. Phys. Quant. Elect. Optoelect. **10**, 1 (2007).
[3] L. Gork'ov and G. Grüner, *Charge Density Waves in Solids* (Elsevier Science, New York, 1989).
[4] H. Requardt *et al.*, Phys. Rev. Lett. **80**, 5631 (1998).
[5] R. Pessoa, S. A. Vitiello, and M. de Koning, Phys. Rev. Lett. **104**, 085301 (2010).
[6] J. Day, O. Syshchenko, and J. Beamish, Phys. Rev. B **79**, 214524 (2009).
[7] I. L. F. Ray and D. J. H. Cockayne, Proc. R. Soc. A **325**, 543 (1971).
[8] M. J. Hytch, J.-L. Putaux, and J.-M. Penisson, Nature (London) **423**, 270 (2003).
[9] G. Vanderschaeve, C. Levade, and D. Caillard, J. Phys. Condens. Matter **12**, 10 093 (2000).
[10] J. R. Patel and A. Authier, J. Appl. Phys. **46**, 118 (1975).
[11] Y. Xin *et al.*, Appl. Phys. Lett. **72**, 2680 (1998).
[12] R. Jones, Mater. Sci. Eng. B **71**, 24 (2000).
[13] I. Robinson *et al.*, J. Phys. D **38**, A7 (2005).
[14] D. L. Bolloc'h *et al.*, Phys. Rev. Lett. **95**, 116401 (2005).
[15] D. Le Bolloc'h *et al.*, High Press. Res. **29**, 635 (2009).
[16] M. Sutton *et al.*, Nature (London) **352**, 608 (1991).
[17] J. Friedel, *Dislocations* (Pergamon Press, Oxford, 1964).
[18] V. L. Jacques *et al.*, Eur. Phys. J. B **70**, 317 (2009).
[19] First experiments were performed at the D2AM beam line (ESRF), F. Livet, G. Rolland, D. Le Bolloc'h, F. Picca and V. L. R. Jacques (private communication).
[20] F. Livet, Acta Crystallogr. Sect. A **63**, 87 (2007).
[21] C. A. Lucas, E. Gartstein, and R. A. Cowley, Acta Crystallogr. Sect. A **45**, 416 (1989).
[22] H. Mimura *et al.*, Nature Phys. **6**, 122 (2009).
[23] T. Martin and A. Koch, J. Synchrotron Radiat. **13**, 180 (2006).
[24] A. Gomez *et al.*, Philos. Mag. **31**, 105 (1975).
[25] P. Thibault *et al.*, Ultramicroscopy **109**, 338 (2009).
[26] M. C. Newton *et al.*, Nature Mater. **9**, 120 (2009).
[27] N. Vaxelaire *et al.*, Nucl. Instrum. Methods Phys. Res., Sect. B **268**, 388 (2010).